

## Ostwald ripening and gravitational equilibrium: Implications for long-term subsurface gas storage

Martin J. Blunt \*

*Department of Earth Science and Engineering, Imperial College London, London SW7 2BP, United Kingdom*



(Received 8 August 2022; accepted 22 September 2022; published 10 October 2022)

The equilibrium configuration of a gas and brine in a porous medium, and the timescales to reach equilibrium, are investigated analytically. If the gas is continuous in the pore space, we have the traditional gravity-capillary transition zone:  $P_c(S_w) = \Delta\rho gz$  where  $P_c$  is the capillary pressure (pressure difference between the gas and aqueous phases),  $S_w$  is the aqueous phase (brine) saturation,  $\Delta\rho = \rho_w - \rho_g$  is the density difference between the phases,  $g$  is the gravitational acceleration, and  $z$  is a vertical distance coordinate increasing upwards, where  $z = 0$  indicates the level where  $P_c = 0$ . However, if the gas is disconnected, as may occur during water influx in carbon dioxide and hydrogen storage, then the nature of equilibrium is different where diffusion through the aqueous phase (Ostwald ripening) maintains a capillary pressure gradient consistent with the thermodynamically-determined brine density as a function of depth:  $P_c = P^*[e^{(V_g\rho_w - m_g)gz/RT} - 1] + \rho_w gz$ , where  $P^*$  is the aqueous phase pressure at  $z = 0$ ,  $V_g$  is the specific molar volume of the gas dissolved in the aqueous phase,  $m_g$  is the molecular mass of the gas,  $R$  is the universal gas constant, and  $T$  is the absolute temperature. The capillary pressure decreases with depth. This means that a deep column of trapped gas cannot be sustained indefinitely. Instead a transition zone forms in equilibrium with connected gas near the top of the formation: its thickness is typically less than 1 m for carbon dioxide, hydrogen, methane or nitrogen in a permeable reservoir. The timescales to reach equilibrium are, however, estimated to be millions of years, and hence do not significantly affect long-term storage over millennia. At the scale of laboratory experiments, in contrast, Ostwald ripening leads to local capillary equilibrium in a few weeks to a year, dependent on the gas considered.

DOI: [10.1103/PhysRevE.106.045103](https://doi.org/10.1103/PhysRevE.106.045103)

### I. INTRODUCTION

Capillary trapping—the isolation of nonwetting phase ganglia surrounded by a wetting, aqueous phase in a porous medium—has been suggested as a rapid and effective way to immobilize carbon dioxide, CO<sub>2</sub>, and other gases over months to years in permeable rock, ensuring that the trapped phase cannot escape [1,2]. In CO<sub>2</sub> storage this is desirable, preventing migration of the gas back into the atmosphere and contributing to climate change. In hydrogen storage, and natural gas recovery, this effect is undesirable as it limits the amount of mobile gas that can be produced and used. However, this analysis ignores transport of dissolved species in the aqueous phase. Brine containing dissolved CO<sub>2</sub> is denser than the unsaturated aqueous phase, and will therefore sink. This can lead to a convective dissolution process which may largely dissolve the CO<sub>2</sub> over thousand-year timescales [3]. This adds to storage security as the CO<sub>2</sub> moves further away from the surface and is no longer in its own phase.

Another phenomenon which has received less attention is Ostwald ripening, where diffusive transport of gas dissolved in the aqueous phase acts to make the local capillary pressure uniform [4–6]. The equilibrium concentration of gas in the aqueous phase is a function of the gas pressure, normally

expressed by Henry’s law:

$$H = \frac{\partial C}{\partial P_g}, \quad (1)$$

where  $C$  is the concentration of gas dissolved in the aqueous phase (in this paper we will express this in units of moles/m<sup>3</sup>),  $P_g$  is the gas pressure (Pa), or, for mixtures, the partial pressure of a specific component in the gaseous phase.  $H$  is the Henry’s law constant with SI units of mol/(m<sup>3</sup>·Pa). If  $H$  is indeed a constant, which we will assume for simplicity here:

$$C = HP_g. \quad (2)$$

The implication of Henry’s law is that in equilibrium, with a constant concentration  $C$ , the gas pressure should also be constant. In capillary trapping, nonwetting gas ganglia are initially formed with different capillary pressures  $P_c = P_g - P_w$  where  $P_w$  is the aqueous phase (water or brine) pressure, governed by the local contact angles, pore structure, and the nature of the displacement process [5,7].

Ostwald ripening refers to diffusion-driven transport to eliminate concentration gradients in the aqueous phase such that the capillary pressure in each gas ganglion (bubble) is constant. In a bulk fluid, this leads to the disappearance of small bubbles (which have smaller radii of curvature and hence higher capillary pressures from the Young-Laplace equation) and the accumulation of all the gas which is not dissolved into a single, large, spherical bubble. In porous media the process is more complex since multiple equilibrium

\*Corresponding author: [m.blunt@imperial.ac.uk](mailto:m.blunt@imperial.ac.uk)

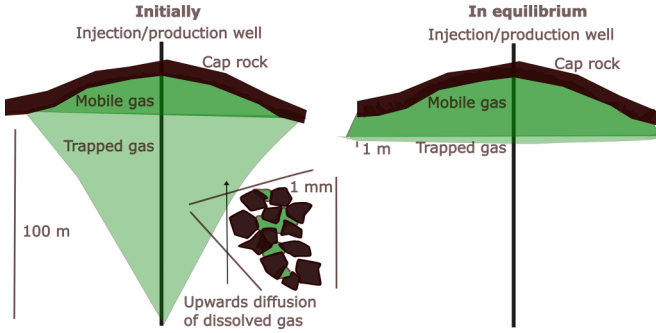


FIG. 1. A schematic of the situation studied in this paper. We consider gas storage and production in a porous medium otherwise saturated with brine (the aqueous phase): this could be a carbon dioxide or hydrogen storage site, or natural gas production. We assume that mobile gas is retained below a low permeability cap rock. Brine influx has led to capillary trapping of gas with an initial distribution of saturation with depth as indicated on the left. Ostwald ripening, facilitated by diffusive transport of gas dissolved in the aqueous phase, leads to a redistribution of trapped gas ganglia (shown in green; the solid is dark brown and brine is white). Higher water pressures with depth lead to larger dissolved concentrations of gas, giving a vertical concentration gradient and an upwards diffusive flux. Eventually a new position of gravity-capillary equilibrium will be reached, Eq. (10), over a timescale given by Eq. (16). This leads to a final saturation profile in equilibrium shown to the right, where gas is trapped and confined to a thin layer below a region of mobile gas.

configurations are possible: small ganglia do not necessarily disappear, as their capillary pressure may decrease as they retreat into large pore spaces, while the growth of larger ganglia is suppressed by the entry capillary pressure required to fill narrow throats between wider pore spaces [4,6].

Previous work has shown that in laboratory experiments of capillary trapping combined with pore-scale imaging, locally trapped ganglia do have different capillary pressures, but with a well-defined peak, or mode value, which suggests that over the timescale of the experiments, from a few hours to a day, Ostwald ripening may be sufficiently rapid to establish partial, but not total, equilibrium over lengths of a few millimeters [5,7,8]. Experiments on two-dimensional micromodels with water and air indicated times to reach equilibrium of order a day over distances of approximately 1–2 mm [4], while fast X-ray imaging detected significant rearrangement of trapped ganglia in sandstone over a period of 30 hours [9]. Other pore-scale imaging experiments have shown the disappearance of small trapped ganglia of air within a few hours [10]. Pore-scale simulations have also demonstrated that multiple configurations of local capillary equilibrium are possible as trapped ganglia rearrange themselves in the pore space [6]. At larger scales, simulations and analytic analysis have been applied to heterogeneous media with spatially varying capillary pressure [11]. Over the scale of meters, local equilibrium is achieved over timescales as long as thousands of years, comparable to the times needed for significant convective dissolution of ganglia [3].

This paper will study the impact of Ostwald ripening on gas storage, shown schematically in Fig. 1. We assume

that influx of brine after injection, or during production, has led to capillary trapping of the gas in the pore space surrounded by the aqueous phase. The contributions of this work will be threefold. Firstly, most work to date has focused on CO<sub>2</sub> storage; here we will also consider the behavior of hydrogen, natural gas (methane), and nitrogen. Secondly, we will demonstrate that in equilibrium trapped ganglia are confined to a small transition zone of less than 1 m below continuous gas, and provide a pore-scale picture of this phenomenon. Thirdly, we will show, however, that the timescales to reach this equilibrium are millions of years. This means that large regions of trapped gas are stable for periods relevant to storage applications.

## II. CAPILLARY-DISSOLUTION-GRAVITY EQUILIBRIUM

This paper is concerned with the configuration of two phases in a porous medium: an aqueous phase and a partially soluble gaseous (or supercritical) phase. Specifically, we will study equilibrium conditions considering buoyancy, capillary forces and phase exchange between gas and liquid (Henry's law) where the mechanism for maintaining equilibrium is diffusion of dissolved species in the aqueous phase, as outlined in Fig. 1. We will assume that the aqueous phase is not flowing, and so we will not investigate convective dissolution, which has already been well studied [3]. We will also ignore mineralization which may play a significant role in permanently sequestering CO<sub>2</sub> in the longterm [12], and assume that the small gradients in concentration do not affect reaction rates.

### A. Equilibrium with continuous gas

To set the scene, first assume that the gaseous phase is connected, defined such that gas can flow in the pore space, indicated as mobile gas in Fig. 1. In this case we achieve the well-known capillary-gravity equilibrium, observed, for instance, in the initial saturation distribution in hydrocarbon reservoirs. We will not plod through the derivation but simply state [13]:

$$\frac{\partial P}{\partial z} = -\rho g, \quad (3)$$

for both gas and aqueous phases, leading to

$$P_c(S_w) = \int_0^z \Delta \rho g dz, \quad (4)$$

where the capillary pressure is traditionally written as a function of the aqueous phase saturation,  $S_w$ ,  $\Delta \rho = \rho_w - \rho_g$  is the density difference between the phases,  $g$  is the acceleration due to gravity, and  $z$  is a vertical coordinate increasing upwards where  $z = 0$  is the free water level defined where  $P_c = 0$ . In CO<sub>2</sub> storage applications, for instance, it is possible for the gas density to vary significantly with depth, particularly if there is a transition from supercritical to gaseous conditions. In many cases, however, we may assume that the phase densities are constant and

$$P_c(S_w) = \Delta \rho g z. \quad (5)$$

This situation leads to a nonequilibrium in dissolved concentration. From Eq. (3)

$$\frac{\partial P_g}{\partial z} = -\rho_g g. \quad (6)$$

From Eqs. (1) and (6), this leads to a concentration gradient:

$$\frac{\partial C}{\partial z} = H \frac{\partial P_g}{\partial z} = -H \rho_g g. \quad (7)$$

Hence there is an upwards diffusive flux of dissolved gas, which then enters the free gaseous phase, leading to a downwards gas flow to maintain capillary-gravity equilibrium. The net gas flux is zero in equilibrium: the upwards movement in the aqueous phase is matched by downwards transport in the continuous gas phase. We will show later that this flux is small at the field scale: the apparent perpetual motion is driven by thermal energy.

### B. Equilibrium with trapped gas

If the gaseous phase is disconnected, this analysis no longer holds, as there is no gas phase flow to offset the effects of the upwards diffusive flux shown in Fig. 1. Normally it is assumed that in vertical cross-section gas can be trapped over an arbitrarily large distance. However, this is not correct at sufficiently long timescales: instead a new position of equilibrium is reached. This is not a constant concentration (and hence capillary pressure) for two reasons. The more significant is that the aqueous phase pressure increases with depth. The second effect is that the dissolution of gas affects the aqueous phase density, which leads to a gradient of gas solubility with  $z$ . We employ a thermodynamic approach to predict the equilibrium dissolved concentration: the probability of a mole of gas to be at a height  $z$  is proportional to  $e^{-\Delta E/RT}$  where  $\Delta E = -\Delta m g z$  is the potential energy penalty [14]. We equate probability with concentration to find:

$$C = C^* e^{\Delta m g z / RT}, \quad (8)$$

where  $C^*$  is the concentration in equilibrium at the free water level: from Eq. (2)  $C^* = H P^*$ .  $R$  is the universal gas constant and  $T$  is the absolute temperature.  $\Delta m$  is change in mass from replacing the volume occupied by one mole of the dissolved gaseous species with brine. This can sound confusing, but is conceptually the increase in mass if we were to replace one mole of gas in solution with the same volume of brine. This is normally calculated using the partial molar volume  $V_g$  which is the volume occupied by one mole of dissolved gas. By definition this has a mass  $m_g$ , the molecular mass of the gas. The same volume of brine has a mass  $V_g \rho_w$  where  $\rho_w$  is the brine density without any dissolved gas present. Hence we can write

$$\Delta m = V_g \rho_w - m_g. \quad (9)$$

The gas pressure in equilibrium is therefore simply  $P_g = C/H$  from Eq. (2). Then using Eqs. (8), (9), and  $P_w = P^* - \rho_w g z$  we can write

$$P_c = P_g - P_w = P^* [e^{(V_g \rho_w - m_g) g z / RT} - 1] + \rho_w g z. \quad (10)$$

Note that this is different from capillary-gravity equilibrium with continuous gas, Eq. (5). This can be seen more clearly

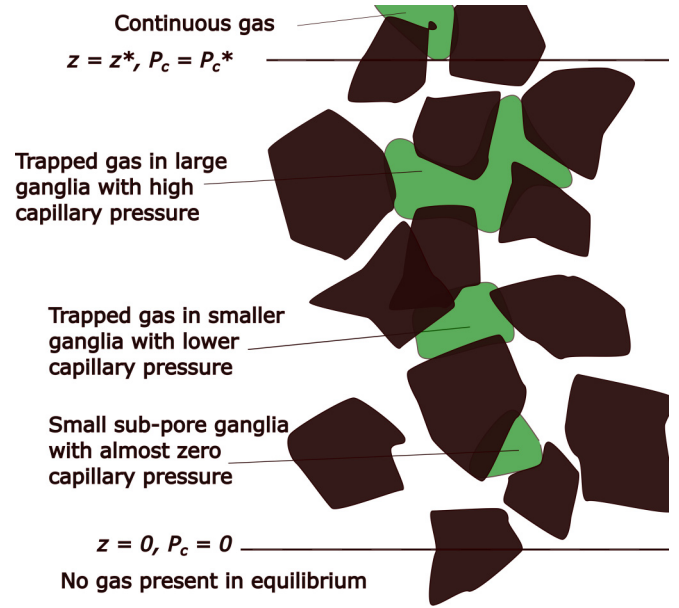


FIG. 2. A schematic of the equilibrium arrangement of trapped phases in equilibrium, Eq. (10), with a transition zone height  $z^*$  given by Eq. (12). Rock is dark brown, gas is green, and brine is white. At  $z = z^*$  continuous gas is first present; below this the gas is trapped. There is a capillary pressure gradient, Eq. (11), such that at  $z = 0$ ,  $P_c = 0$  and it is no longer possible to retain trapped phases if we assume that the rock is water-wet. We will see a transition in saturation. It is hypothesized that larger multiple pore trapped ganglia are seen near  $z = z^*$  with a high capillary pressure—the menisci are present in small throats, the restrictions between pores. Lower we see smaller ganglia at a lower capillary pressure. Just above  $z = 0$  sub-pore ganglia may be present, retained in roughness of the pore space, or in patches where, locally, the contact angle is higher.

if we look at the capillary pressure gradient under the assumption that  $|(V_g \rho_w - m_g) g z / RT| \ll 1$  (for the examples we consider the magnitude of this term is of order  $10^{-4} z$  or lower):

$$\frac{\partial P_c}{\partial z} = \rho_w g + \frac{P^* (V_g \rho_w - m_g) g}{RT}. \quad (11)$$

### C. Pore-scale picture

A schematic of the pore-scale picture of equilibrium is provided in Fig. 2. Imagine that at some height  $z^*$  the gas is first connected with an entry capillary pressure  $P_c^*$ . In equilibrium, there will be a transition zone below the connected gas containing trapped ganglia to  $z = 0$  where the capillary pressure is zero; we do not expect to see ganglia below this level as it would require the gas to reside in the pore space with a negative capillary pressure, which is difficult to achieve if the rock is water-wet. There will be a trend in saturation, from 0 at  $z = 0$  to  $S_{gr}$ , the original residual saturation, just at  $z^*$ , before the gas is connected. This saturation trend has not been studied previously: it represents the amount of residual trapping possible for a given imposed capillary pressure.

It is hypothesized that near  $z = z^*$  large multiple-pore ganglia will be seen, with menisci present in small throats (the restrictions between pores) with a high local capillary

pressure. Lower in the transition zone, smaller single-pore ganglia with a lower capillary pressure will be observed. Near  $z = 0$  the capillary pressure is close to zero. Here trapped gas can only be retained in small sub-pore ganglia, contained in roughness, or in regions with locally a higher than average contact angle. Such small ganglia have been observed in imaging experiments [15–18]. This picture needs to be confirmed directly at the pore scale since it assumes, contrary to the situation in a bulk fluid, that higher capillary pressures are associated with larger ganglia, while smaller ganglia have lower capillary pressures. Regardless of the pore-scale configuration of fluid, trapped ganglia will be confined in equilibrium to a narrow region below the connected gas. To recap, at the mesoscale we will see a variation in saturation with depth from  $S_g = S_{gr}$  at  $z = z^*$  to  $S_g = 0$  at  $z = 0$ .

The height of the transition zone  $z^*$  is found from Eq. (11):

$$z^* = \frac{P_c^*}{\rho_w g + P^*(V_g \rho_w - m_g)g/RT}. \quad (12)$$

In summary, trapped ganglia will be confined to a small region below where the gas is connected in the pore space. This means that capillary trapping cannot retain gas over extensive vertical distances in the long term. While this may appear to limit the effectiveness of capillary trapping, we do need to assess the rate at which equilibrium is reached, which is quantified in the next section.

### III. DIFFUSIVE FLUXES AND TIMES TO REACH EQUILIBRIUM

This section will assess the diffusive flux of dissolved species to estimate the timescales to reach an equilibrium distribution of phases, as described by Eq. (10).

The vertical flux,  $F$ , of dissolved material is found from Fick's first law:

$$F = -D \frac{\partial C}{\partial z}, \quad (13)$$

where  $D$  is the diffusion coefficient; this is an effective value in the porous medium which is smaller than that measured in bulk solution. Let us imagine a situation where gas is capillary trapped in a tall vertical column at an approximately constant capillary pressure, while the brine is stagnant (or at least there is no vertical flow of the aqueous phase), as indicated in Fig. 1. In this case the gas pressure is the water pressure plus the constant capillary pressure. Hence using Eq. (1):

$$\frac{\partial C}{\partial z} = H \frac{\partial P_g}{\partial z} = -H \rho_w g, \quad (14)$$

and from Eq. (13):

$$F = DH \rho_w g. \quad (15)$$

Assuming that the flux remains constant we can estimate the timescale for ganglia deep in the formation to disappear through Ostwald ripening. If initially the trapped saturation is  $S_{gr}$  in a rock of porosity  $\phi$  over a height  $h$  with a density  $\rho_g$  and molecular mass  $m_g$ , then the moles of free gas per unit horizontal cross-sectional are  $h\phi S_{gr} \rho_g / m_g$ . From Eq. (15), the time  $T$  for the diffusive flux to remove the trapped gas

completely is

$$T = \frac{h\phi S_{gr} \rho_g}{DH \rho_w g m_g}. \quad (16)$$

The other situation we will consider is the timescale for local equilibrium after a laboratory experiment. Here the concentration gradients are caused by differences in local capillary pressure in the trapped ganglia: the ganglia rearrange in the pore space to make the capillary pressure locally constant. We assume a representative capillary pressure  $P_c^* = 2\sigma/r$  where  $\sigma$  is the interfacial tension between the gas and aqueous phases while  $r$  is a typical throat radius. If we consider the achievement of equilibrium over a length scale  $l$  then the concentration gradients are of magnitude:

$$\frac{\partial C}{\partial z} \approx \frac{HP_c^*}{l} = \frac{2H\sigma}{lr}, \quad (17)$$

and using the same approach as above, we can estimate a typical timescale for equilibrium over a length  $l$  as

$$t = \frac{l^2 r \phi S_{gr} \rho_g}{2DH \sigma m_g}. \quad (18)$$

This is likely to overestimate the equilibrium time since this allows complete removal or movement of the trapped gas; in reality only a fraction of the gas volume needs to move to achieve equilibrium.

It is possible that at the pore scale, the rearrangement of ganglia could lead to reconnection of the gas phase. In this case, transport will be much faster to reach equilibrium; however, as the gas moves upwards and the saturation decreases it will again disconnect reaching a new position of local equilibrium, as seen experimentally and in modeling studies [11]. In the end, the time to reach equilibrium will be determined principally by diffusive transport between trapped gas ganglia, as outlined here.

### IV. APPLICATION TO PRODUCTION AND STORAGE

We will now estimate typical transition zone heights in equilibrium, containing trapped gas, Eq. (12), as well as the diffusive fluxes and Ostwald ripening timescales, Eqs. (16) and (18) for four examples: CO<sub>2</sub> (for storage applications), hydrogen (for storage and withdrawal), methane (as a cushion gas, during natural gas production with an aquifer drive, or a solution gas drive in an oilfield), and nitrogen (representing trapped air near the water table, or its use as a cushion gas in the storage of other gases).

The properties we assume are provided in Table I. Note that we only present here approximate calculations and so we have not attempted to make accurate corrections for temperature, pressure, and salinity. The temperature and pressure conditions are  $T = 50^\circ\text{C}$  (323 K) and  $P^* = 10$  MPa, respectively. We assume that the initial trapped saturation  $S_{gr} = 0.3$  and the porosity  $\phi = 0.2$ . We consider  $h = 100$  m to represent a significant zone of trapped gas as illustrated in Fig. 1. We take  $l = 1$  mm for pore-scale equilibrium in laboratory experiments. To estimate the diffusion coefficients in a porous medium, we multiply measurements made in bulk by the porosity to account for the restricted transport in the pore space. For Henry's constants, we use values in pure water

TABLE I. Data for the calculation of transition zone heights, Eq. (19), and timescales for equilibrium at the pore and field scales, Eqs. (18) and (16), respectively, for carbon dioxide CO<sub>2</sub>, hydrogen H<sub>2</sub>, methane CH<sub>4</sub>, and nitrogen N<sub>2</sub>. Density data from [21,22], interfacial tensions from [23–25], partial molar volumes from [26–28], diffusion data from [22,29], and Henry's constants from [19].  $\phi = 0.2$ ,  $S_{gr} = 0.3$ ,  $T = 323\text{K}$ ,  $P^* = 10^7\text{ Pa}$ ,  $\rho_w = 1050\text{ kg.m}^{-3}$ ,  $l = 10^{-3}\text{ m}$ ,  $h = 100\text{ m}$ ,  $r = 2.4 \times 10^{-5}\text{ m}$ ,  $R = 8.314\text{ J.K}^{-1}.\text{mol}^{-1}$ , and  $g = 9.81\text{ m.s}^{-2}$ .

Property/Gas	CO <sub>2</sub>	H <sub>2</sub>	CH <sub>4</sub>	N <sub>2</sub>
Density $\rho_g$ [kg.m <sup>-3</sup> ]	400	7.1	68	112
Interfacial tension with brine $\sigma$ [Pa.s]	0.0349	0.07	0.057	0.0635
Molecular mass $m_g$ [kg.mol <sup>-1</sup> ]	0.044	0.002	0.016	0.028
Partial molar volume $V_g$ [m <sup>3</sup> .mol <sup>-1</sup> ]	$3.5 \times 10^{-5}$	$2.5 \times 10^{-5}$	$2.5 \times 10^{-5}$	$4 \times 10^{-5}$
Diffusion coefficient $D$ [m <sup>2</sup> .s <sup>-1</sup> ]	$7.2 \times 10^{-10}$	$1.8 \times 10^{-9}$	$6.4 \times 10^{-10}$	$7.0 \times 10^{-10}$
Henry's constant $H$ [mol.m <sup>-3</sup> .Pa <sup>-1</sup> ]	$1.8 \times 10^{-4}$	$6.9 \times 10^{-6}$	$9.2 \times 10^{-6}$	$4.7 \times 10^{-6}$
Transition zone height $z^*$ [m]	0.29	0.52	0.44	0.50
Timescale for pore-scale equilibrium $t$ [s]	$1.5 \times 10^6$	$3 \times 10^6$	$9 \times 10^6$	$1.4 \times 10^7$
Timescale for field equilibrium $t$ [s]	$4 \times 10^{13}$	$2 \times 10^{14}$	$4 \times 10^{14}$	$7 \times 10^{14}$

corrected for temperature [19], but do not account for the salting-out effect, which lowers the solubility of gases in a high salinity brine. For the equilibrium transition zone, Eq. (12), as above, we take  $P_c^* = 2\sigma/r$  where  $r = 24\ \mu\text{m}$  based on Bentheimer sandstone [13,20]. We assume a brine density  $\rho_w = 1,050\text{ kg.m}^{-3}$ .

In summary, to find the estimated values for the equilibrium transition zone thickness, Eq. (12), we use the expression for capillary pressure to write:

$$z^* = \frac{2\sigma}{r\rho_w g} \cdot \frac{1}{1 + P^*(V_g - m_g/\rho_w)/RT}. \quad (19)$$

The results presented in Table I lead to the following observations:

(1) In equilibrium, density variations with depth and Ostwald ripening lead to a transition zone height—the region containing trapped gas ganglia in equilibrium—of less than 1 m in all cases. This means that trapped gas cannot be retained indefinitely in a vertical column of arbitrary height.

(2) The timescales to reach equilibrium are, however, exceptionally long. For reference, 1 million years is  $3 \times 10^{13}\text{ s}$ : for the gases studied, equilibrium over around 100 m takes several million years. While this is achievable on geological timescales, the redistribution of trapped ganglia in gravitational equilibrium is negligible on the timescales of interest for storage and withdrawal: years to millennia. This means that other effects, including dissolution and convective mixing, reaction, mineralization, and bacterial degradation [30], will be more significant than Ostwald ripening.

(3) In contrast, at the laboratory scale, Ostwald ripening is faster with complete equilibrium achieved at the scale of 1 mm in around two to four weeks (for CO<sub>2</sub> and hydrogen) and up to one year (methane and nitrogen). This is likely to be an over-estimate of the time required since it allows sufficient transport for complete removal of the trapped phase. Experiments that study hydrogen and CO<sub>2</sub> trapping imaging may capture a state in partial equilibrium, with rearrangement of trapped ganglia due to Ostwald ripening potentially observable at the porescale over days to weeks. For nitrogen

and methane, though, longer times are required to reach equilibrium and the pore-scale configuration of trapped phases observed in imaging experiments is unlikely to be significantly affected by Ostwald ripening.

## V. CONCLUSIONS

This paper has presented an analytical analysis of Ostwald ripening with application to underground gas storage and production. The equilibrium distribution of phases has been derived, including an expression for the capillary pressure and transition zone height for trapped gas ganglia. This is different from the normal capillary-gravity equilibrium associated with connected phases and arises from the redistribution of gas by Ostwald ripening resulting in a vertical saturation profile of the trapped phase below continuous gas. A pore-scale picture and explanation of the phenomenon was provided. The transition zone is estimated to less than 1 m in a permeable formation for all of the four gases studied: carbon dioxide, hydrogen, methane, and nitrogen.

The timescales to reach equilibrium were estimated. In all cases, millions of years would be required to establish equilibrium. While this may be relevant for geological processes, in the context of storage and production, with timescales of years to millennia, the impact of diffusive fluxes on removing a deep column of trapped gas is negligible. On the other hand, at the scale of laboratory experiments, Ostwald ripening may establish partial equilibrium for hydrogen and carbon dioxide over days to order of a month.

Further work is required to study the redistribution dynamics of trapped phases to test the pore-scale conceptualization presented here. Imaging experiments could be performed to observe changes in the configuration of trapped ganglia of hydrogen and carbon dioxide due to Ostwald ripening building on previous work [6,9].

## ACKNOWLEDGMENTS

The author thanks Shell under the Digital Rocks Programme for funding this work, and for Dr. Steffen Berg for first suggesting the work on this problem.

- [1] S. M. Benson and D. R. Cole, CO<sub>2</sub> sequestration in deep sedimentary formations, *Elements* **4**, 325 (2008).
- [2] S. Krevor, M. J. Blunt, S. M. Benson, C. H. Pentland, C. Reynolds, A. Al-Menhali, and B. Niu, Capillary trapping for geologic carbon dioxide storage – from pore scale physics to field scale implications, *Int. J. Greenhouse Gas Control* **40**, 221 (2015).
- [3] J. A. Neufeld, M. A. Hesse, A. Riaz, M. A. Hallworth, H. A. Tchelepi, and H. E. Huppert, Convective dissolution of carbon dioxide in saline aquifers, *Geophys. Res. Lett.* **37**, L22404 (2010).
- [4] K. Xu, R. Bonnecaze, and M. Balhoff, Egalitarianism among Bubbles in Porous Media: An Ostwald Ripening Derived Anti-coarsening Phenomenon, *Phys. Rev. Lett.* **119**, 264502 (2017).
- [5] C. Garing, J. A. de Chalendar, M. Voltolini, J. B. Ajo-Franklin, and S. M. Benson, Pore-scale capillary pressure analysis using multi-scale x-ray micromotography, *Adv. Water Resour.* **104**, 223 (2017).
- [6] J. A. de Chalendar, C. Garing, and S. M. Benson, Pore-scale modelling of Ostwald ripening, *J. Fluid Mech.* **835**, 363 (2018).
- [7] M. G. Andrew, B. Bijeljic, and M. J. Blunt, Pore-by-pore capillary pressure measurements using x-ray microtomography at reservoir conditions: Curvature, snap-off, and remobilization of residual CO<sub>2</sub>, *Water Resour. Res.* **50**, 8760 (2014).
- [8] M. G. Andrew, B. Bijeljic, and M. J. Blunt, Pore-scale imaging of trapped supercritical carbon dioxide in sandstones and carbonates, *Int. J. Greenhouse Gas Control* **22**, 1 (2014).
- [9] C. Garing, M. Voltolini, J. B. Ajo-Franklin, and S. M. Benson, Pore-scale evolution of trapped CO<sub>2</sub> at early stages following imbibition using micro-ct imaging, *Energy Procedia* **114**, 4872 (2017).
- [10] Y. Gao, T. Sorop, N. Brussee, H. van der Linde, A. Coorn, M. Appel, and S. Berg, Advanced digital-SCAL measurements of gas trapped in sandstone, paper SCA2022-043, in *Proceedings of SCA Annual Meeting, Austin, Texas* (Society of Core Analysts, New Brunswick, Canada, 2022).
- [11] Y. Li, C. Garing, and S. M. Benson, A continuum-scale representation of Ostwald ripening in heterogeneous porous media, *J. Fluid Mech.* **889**, A14 (2020).
- [12] *National Academies of Sciences, Medicine, Negative Emissions Technologies and Reliable Sequestration: A Research Agenda* (The National Academies Press, Washington, DC, 2019).
- [13] M. J. Blunt, *Multiphase Flow in Permeable Media: a Pore-Scale Perspective* (Cambridge University Press, Cambridge, UK, 2017).
- [14] L. D. Landau and E. M. Lifshitz, *Statistical Physics* (Elsevier, Amsterdam, 1959).
- [15] T. Pak, I. B. Butler, S. Geiger, M. I. J. van Dijke, and K. S. Sorbie, Droplet fragmentation: 3D imaging of a previously unidentified pore-scale process during multiphase flow in porous media, *Proc. Natl. Acad. Sci. USA* **112**, 1947 (2015).
- [16] K. Singh, H. Menke, M. Andrew, Q. Lin, C. Rao, M. J. Blunt, and B. Bijeljic, Dynamics of snap-off and pore-filling events during two-phase flow in permeable media, *Sci. Rep.* **7**, 5192 (2017).
- [17] A. AlRatrou, M. J. Blunt, and B. Bijeljic, Spatial correlation of contact angle and curvature in pore-space images, *Water Resour. Res.* **54**, 6133 (2018).
- [18] K. Singh, T. Bultreys, A. Q. Raeini, M. Shams, and M. J. Blunt, New type of pore-snap-off and displacement correlations in imbibition, *J. Colloid Interface Sci.* **609**, 384 (2022).
- [19] R. Sander, Compilation of Henry's law constants (version 4.0) for water as solvent, *Atmos. Chem. Phys.* **15**, 4399 (2015).
- [20] Q. Lin, B. Bijeljic, R. Pini, M. J. Blunt, and S. Krevor, Imaging and measurement of pore-scale interfacial curvature to determine capillary pressure simultaneously with relative permeability, *Water Resour. Res.* **54**, 7046 (2018).
- [21] A. Bahadori, H. B. Vuthaluru, and S. Mokhatab, New correlations predict aqueous solubility and density of carbon dioxide, *Int. J. Greenhouse Gas Control* **3**, 474 (2009).
- [22] Engineering toolbox, <https://www.engineeringtoolbox.com/>.
- [23] Y. F. Chow, G. C. Maitland, and J. M. Trusler, Interfacial tensions of the (CO<sub>2</sub> + N<sub>2</sub> + H<sub>2</sub>O) system at temperatures of (298 to 448)K and pressures up to 40MPa, *J. Chem. Thermodyn.* **93**, 392 (2016).
- [24] K. Kashefi, L. M. Pereira, A. Chapoy, R. Burgass, and B. Tohidi, Measurement and modelling of interfacial tension in methane/water and methane/brine systems at reservoir conditions, *Fluid Phase Equilib.* **409**, 301 (2016).
- [25] M. Hosseini, J. Fahimpour, M. Ali, A. Keshavarz, and S. Iglauer, H<sub>2</sub>-brine interfacial tension as a function of salinity, temperature, and pressure; implications for hydrogen geo-storage, *J. Pet. Sci. Eng.* **213**, 110441 (2022).
- [26] S. Mao and Z. Duan, A thermodynamic model for calculating nitrogen solubility, gas phase composition and density of the N<sub>2</sub>-H<sub>2</sub>O-NaCl system, *Fluid Phase Equilib.* **248**, 103 (2006).
- [27] T. Zhou and R. Battino, Partial molar volumes of 13 gases in water at 298.15 K and 303.15 K, *J. Chem. Eng. Data* **46**, 331 (2001).
- [28] M. McBride-Wright, G. C. Maitland, and J. P. M. Trusler, Viscosity and density of aqueous solutions of carbon dioxide at temperatures from (274 to 449) K and at pressures up to 100 MPa, *J. Chem. Eng. Data* **60**, 171 (2015).
- [29] S. P. Cadogan, G. P. Maitland, and J. P. M. Trusler, Diffusion coefficients of CO<sub>2</sub> and N<sub>2</sub> in water at temperatures between 298.15 K and 423.15 K at pressures up to 45 MPa, *J. Chem. Eng. Data* **59**, 519 (2014).
- [30] R. L. Tyne, P. H. Barry, M. Lawson, D. J. Byrne, O. Warr, H. Xie, D. J. Hillemonds, M. Formolo, Z. M. Summers, B. Skinner, J. M. Eiler, and C. J. Ballentine, Rapid microbial methanogenesis during CO<sub>2</sub> storage in hydrocarbon reservoirs, *Nature* **600**, 670 (2021).